Multiple-scattering x-ray-absorption fine-structure Debye-Waller factor calculations

A. V. Poiarkova and J. J. Rehr
Department of Physics, University of Washington, Seattle, Washington 98195-1560
(Received 4 May 1998)

An efficient local equation-of-motion method is introduced for calculations of the mean-square half-path-length fluctuations σ_j^2 in multiple-scattering x-ray-absorption fine-structure Debye-Waller factors in aperiodic systems. Given a few local force constants, the method yields σ_j^2 via projected densities of modes or via the displacement-displacement correlation function in real time, over a few vibration cycles. The calculation scales linearly with the system size and does not rely on any symmetry considerations. Sample applications are presented for crystalline Cu and Ge, and zinc tetraimidazole. [S0163-1829(99)12601-8]

I. INTRODUCTION

A. Background

In the recent years x-ray-absorption fine-structure (XAFS) analysis has become an important and widely used technique for determining the local microscopic structure of complex and disordered materials. The structural information it provides includes average near-neighbor distances R, their mean-square fluctuations σ_R^2, and coordination numbers N_R. The quantities σ_R^2 which appear in the XAFS Debye-Waller (DW) factor are crucial to the success of the modern theory of XAFS. The DW factor accounts for thermal and structural disorder and generally governs the ''melting'' of the XAFS oscillations with respect to increasing temperature and their decay with respect to increasing photoelectron energy. In practice, the DW factors of the many multiple-scattering (MS) terms in the XAFS signal can significantly complicate the analysis.[1–3] To overcome this difficulty we present here a general equation-of-motion (EM) method for calculating these DW factors in terms of a few local force constants in arbitrary aperiodic systems. This method is a significant improvement over conventional isotropic models such as the correlated Einstein and Debye models, and offers a number of advantages over full lattice dynamical calculations for aperiodic systems. Although there is no advantage for periodic systems, the method is fast and is shown to give comparable results for XAFS DW factors.

The purpose of this paper is to discuss the theory and calculation of thermal XAFS DW factors, with emphasis on their physical interpretation in terms of the local dynamical vibrational structure. Structural disorder can be included by an additional multiplicative DW factor, independent of temperature,[4] for example, using the cumulant expansion.[3,4] In particular, we develop here a method to calculate the mean-square half-path-length fluctuation $\sigma_j^2(T)$ from thermal motion for a general scattering path j in the harmonic approximation, given a few local parameters in a valence force field (VFF) model. Many other studies of XAFS DW factors have been conducted previously[4–7] and attempts have been made to obtain effective σ_R^2 using experimental vibrational spectra,[8] but they are usually limited to the single-scattering (SS) case. Our treatment differs from the approach of Benfatto *et al.*[9] in that no explicit matrix inversion is required.

We find that σ_j^2 depends primarily on the vibrational structure in the local environment around a scattering path. The locality of σ_j^2 allows us to address the problem of its calculation in terms of small clusters of atoms, without the use of periodic boundary conditions or any symmetry considerations. Thus our approach can be applied to general materials, including amorphous and irregular lattices, as in biological complexes. This also means that for complicated polyatomic structures, one needs an accurate model of interatomic interactions only in the immediate vicinity of a scattering center and an effective (or average) force field for interactions between further atoms. As will be shown for the case of molecular zinc tetraimidazole, this prescription significantly reduces the number of force constants needed in the calculations. We will also show that it is possible to achieve a much better agreement with experiment using just a few more parameters than in conventional isotropic models such as the correlated Einstein and Debye approximations. The sensitivity of σ_j^2 to displacement-displacement correlations suggests that XAFS can be of significant value in testing the validity of a given lattice dynamical model. This also raises the possibility of solving the ''inverse problem,'' that is, of deducing microscopic force constants directly from experimental XAFS spectra. Since the numerical implementation of the EM method is compatible with FEFF (Ref. 2) and fitting codes such as FEFFIT,[3,10] the unknown force constants and, hence, local vibrational densities of states (VDOS) can be fitted to experiment. We plan to address this further in future work. For the present paper, however, we will simply assume that a VFF model is known *a priori*. To illustrate the method, sample applications will be presented for molecular zinc tetraimidazole, as well as for crystalline Cu and Ge, which were used for testing purposes.

In this work the DW factor $\exp[-W_j(k)]$ for a given scattering path of total length $2r_j$ is defined by the thermal and configurational average of the oscillatory part of the XAFS signal:

$$\langle e^{i2kr_j}\rangle = e^{i2kR_j}e^{-W_j(k)}, \tag{1}$$

where the index j corresponds to the jth scattering path. Curved-wave effects on the DW factors are usually negligible and will be ignored here.[11] We also neglect anharmonic corrections. In the weak-disorder limit (or harmonic approxi-

mation), this DW factor is a Gaussian, $W_j(k)=2k^2\sigma_j^2$, where $\sigma_j^2=\langle(r_j-R_j)^2\rangle$ is the mean-square variation in the effective or half-path length $R_j=\langle r_j\rangle$ appearing in the standard XAFS equation

$$\chi(k)=\sum_j \frac{N_j S_0^2}{kR_j^2}|f_j^{\rm eff}(k,R_j)| \times \sin[2kR_j+\phi_j(k)]e^{-2R_j/\lambda}e^{-2\sigma_j^2k^2}. \quad (2)$$

Here the sum runs over all unique scattering paths j (i.e., both SS and MS paths) of degeneracy N_j, $f_j^{\rm eff}(k,R_j)$ is the effective curved-wave backscattering amplitude, S_0^2 is a many-body amplitude reduction factor, $\phi_j(k)$ is the net phase shift, $k=[2(E-E_F)]^{1/2}$ is the wave number measured from threshold E_F, and λ is the photoelectron mean free path.

B. XAFS Debye-Waller factors

To better understand the nature of MS DW factors it is useful to examine their origin. The XAFS spectrum χ is defined as the normalized, oscillatory part of the x-ray-absorption coefficient μ, i.e., $\chi=(\mu-\mu_0)/\mu_0$, where μ_0 is the smooth atomic-background absorption. According to XAFS theory χ can be expressed as a thermal average[1]

$$\chi(k)=\mathrm{Im}\left\langle \sum_j \frac{N_j S_0^2 f_j^{\rm eff}(k,r_j)}{kr_j^2} e^{i(2kr_j+2\delta_c)-2r_j/\lambda}\right\rangle, \quad (3)$$

where δ_c is central atom phase shift and r_j is a dynamical variable equal to the instantaneous effective length of a scattering path j. Assuming small disorder and neglecting curved-wave effects from the r_j dependence of $f_j^{\rm eff}$, $\exp(-2r_j/\lambda)$, and $1/r_j^2$ we have

$$\chi(k)=\mathrm{Im}\sum_j \frac{N_j S_0^2 f_j^{\rm eff}(k,R_j)}{kR_j^2} e^{i2\delta_c-2R_j/\lambda}\langle e^{i2kr_j}\rangle, \quad (4)$$

where the thermal average is given by

$$\langle e^{i2kr_j}\rangle=\frac{\mathrm{Tr}\ e^{-\beta H}e^{i2kr_j}}{\mathrm{Tr}\ e^{-\beta H}}. \quad (5)$$

Here H is the lattice Hamiltonian and $\beta=1/k_BT$. Now let $\vec{u}_i$ be the displacement from equilibrium of the ion at site i, so that neglecting terms of order u_i^2, the effective path length for a scattering path j with n_j scattering legs is

$$r_j\simeq R_j+\frac{1}{2}\sum_{i=1}^{n_j}(\vec{u}_i-\vec{u}_{i+})\cdot\hat{R}_{ii+}. \quad (6)$$

Here $i+\equiv i+1$, $i=n_j+1$ corresponds to site $i=1$, $R_j\equiv(1/2)\Sigma_i R_{ii+}$ is, as before, the effective equilibrium path length, R_{ii+} is the equilibrium interatomic distance between atoms i and $i+$, and $\hat{R}_{ii+}$ is the corresponding directing unit vector. From the Born-Oppenheimer approximation, the ion motion can be regarded as stationary during a transition. Hence, the thermal averages are to be carried out in the *ground state* prior to x-ray absorption, rather than in relaxed final states. Now, for any harmonic Hamiltonian or Gaussian disorder one has the exact result[12]

$$\left\langle \exp\left(i2k\sum_i (\vec{u}_i-\vec{u}_{i+})\cdot\hat{R}_{ii+}\right)\right\rangle = e^{-2k^2\sigma_j^2}, \quad (7)$$

where σ_j^2 denotes the mean-square fluctuation in the effective path length R_j:

$$\sigma_j^2=\frac{1}{4}\left\langle\left[\sum_{i=1}^{n_j}(\vec{u}_i-\vec{u}_{i+})\cdot\hat{R}_{ii+}\right]^2\right\rangle. \quad (8)$$

For example, in the SS case of two atoms at sites $\vec{0}$ and $\vec{R}$,

$$\sigma_R^2=\langle[(\vec{u}_R-\vec{u}_0)\cdot\hat{R}]^2\rangle =\langle(\vec{u}_R\cdot\hat{R})^2\rangle+\langle(\vec{u}_0\cdot\hat{R})^2\rangle-2\langle(\vec{u}_R\cdot\hat{R})(\vec{u}_0\cdot\hat{R})\rangle. \quad (9)$$

Thus, if one neglects the variation of all terms but the rapidly varying oscillatory function in Eq. (3) and assumes small harmonic displacements, $\sigma_j/R_j\ll 1$, Eq. (2) is recovered.

Equation (8) shows that σ_j^2 is not merely a sum of mean-square displacements $\langle u_i^2\rangle$ at scattering sites but also includes the displacement-displacement correlation terms $\langle u_{i\alpha}u_{k\beta}\rangle$, where α and β denote Cartesian indices x, y, and z. These correlations decay algebraically with distance and are such that only modes contributing to motion along a bond path are important. Therefore, in contrast to the mean-square displacement $\langle u_{i\alpha}^2\rangle$ which appears in the x-ray-diffraction DW factor, σ_j^2 depends on fluctuations in pair distances and thus provides a direct measure of the displacement-displacement correlation function. As will be shown below σ_j^2 is also related to a certain projected local VDOS and therefore is determined by the local vibrational structure.

We will discuss our results in comparison with two isotropic models commonly used for calculations of the XAFS DW factors, namely, the correlated Debye (CD) and correlated Einstein (CE) models.[5] Such an isotropic approach may not be able to provide an adequate description of vibrational properties for heterogeneous structures and, hence, can lead to poor agreement with experimental data. Therefore, it is important to have a more general microscopic approach to the DW factor calculations which could be effectively applied to SS as well as MS terms.

II. EQUATION-OF-MOTION METHOD

A. Formalism

The approach used in the present study is a finite temperature EM method introduced by Rehr and Alben[6] and Beeman and Alben[13] for calculation of the total vibrational density of states and related quantities. This technique builds in Bose-Einstein statistics and allows one to calculate XAFS $\sigma_j^2(T)$ either in real time or in the frequency domain. The EM method has a number of advantages. For example, it is very efficient for large systems since diagonalization of huge matrices is not required and the calculation time scales linearly with the size of a cluster.

The EM method is based on solving $3N$ coupled Newton's equations of motion with initial conditions depending uniquely on a given scattering path, where N is the number of atoms in the cluster. Regarding the total potential energy Φ of the crystal lattice as a function of the atomic displace-

ments $\vec{u}_i$ from their equilibrium positions, and making use of a harmonic approximation, one obtains the equations of motion[12]

$$\frac{d^2Q_{i\alpha}(t)}{dt^2} = -\sum_{k\beta} D_{i\alpha,k\beta}Q_{k\beta}. \tag{10}$$

Here $\vec{Q}_i = \vec{u}_i\sqrt{M_i}$, M_i is the mass of the atom at site i, and $D_{i\alpha,k\beta} = \Phi_{i\alpha,k\beta}/\sqrt{M_iM_k}$ is the dynamical matrix of order $3N\times 3N$ where $\Phi_{i\alpha,k\beta}$ are the second derivatives of the potential energy with respect to the atomic displacements $u_{i\alpha}$ and $u_{k\beta}$ taken at the equilibrium configuration. Upon substituting the canonical displacement vectors $\vec{Q}_i$ expanded in normal coordinates q_λ,

$$\vec{Q}_i = \sum_\lambda \vec{\epsilon}_i(\lambda)q_\lambda, \tag{11}$$

into the definition of the mean-square fluctuation in the effective path length R_j, these equations of motion lead to a standard eigenvalue problem for the normal modes:

$$\omega_\lambda^2\epsilon_{i\alpha}(\lambda) = \sum_{k\beta} D_{i\alpha,k\beta}\epsilon_{k\beta}(\lambda). \tag{12}$$

Then evaluating the thermal average using Bose-Einstein statistics,

$$\omega^2\langle q_\lambda\rangle^2 = \left\langle n(\omega_\lambda)+\frac{1}{2}\right\rangle\hbar\omega_\lambda = \frac{\hbar\omega_\lambda}{2}\coth\frac{\hbar\omega_\lambda\beta}{2}, \tag{13}$$

one obtains a frequency domain formula for σ_j^2:

$$\sigma_j^2(T) = \frac{\hbar}{2\mu_j}\int_0^{\omega_{max}}\frac{d\omega}{\omega}\rho_j(\omega)\coth\frac{\beta\hbar\omega}{2}. \tag{14}$$

Here μ_j is an effective reduced mass for scattering path j that ensures normalized initial conditions, $\beta = 1/k_BT$, $\omega_{max} \gtrsim z\sqrt{k_1/\mu_1}$ is maximum frequency of the lattice motion, z is the coordination number, k_1 is the central first-neighbor force constant, μ_1 is reduced mass of the scattering center and its first neighbor, and

$$\rho_j(\omega) \equiv \sum_\lambda |\langle\lambda|Q_j(0)\rangle|^2\delta_\Delta(\omega-\omega_\lambda)$$
$$= \frac{2}{\pi}\int_0^{t_{max}}\langle Q_j(t)|Q_j(0)\rangle\cos\omega t e^{-\varepsilon t^2}dt \tag{15}$$

is the projected VDOS contributing to σ_j^2. In the time integration $\varepsilon = 3/t_{max}^2$ and $t_{max} = \sqrt{6}/(\omega_{max}\Delta)$ are cutoff parameters that fix the net spectral resolution width Δ (typically 5% of the bandwidth), δ_Δ is a narrow δ-like function of width Δ, and $\langle Q_j(t)|Q_j(0)\rangle = \Sigma_{i,\alpha}^{n_j}Q_{i\alpha}(t)Q_{i\alpha}(0)$ is the displacement-displacement autocorrelation function. The displacement state vector $|Q_j(t)\rangle$ is determined by integrating the equations of motion (10) numerically using a two-step difference equation approximation with initial velocities set to zero and initial displacements $|Q_j(0)\rangle$. The specific form of the initial displacements depends on the scattering path, as defined below. The cutoff parameters are introduced for efficiency in the calculation, and focus on the local environment by cutting off long-distance behavior.

By substituting Eq. (15) for $\rho_j(\omega)$ into Eq. (14) and evaluating the Fourier transform, one obtains an equivalent real time expression for $\sigma_j^2(T)$:

$$\sigma_j^2(T) = \frac{\hbar}{\mu_j\pi}\int_0^{t_{max}}dt\langle Q_j(t)|Q_j(0)\rangle$$
$$\times\ln\left[\left(2\sinh\frac{\pi t}{\beta\hbar}\right)^{-1}\right]e^{-\varepsilon t^2}. \tag{16}$$

Therefore, in principle, it is not necessary to determine $\rho_j(\omega)$ as an intermediate step, and $\sigma_j^2(T)$ can be explicitly calculated from the corresponding displacement-displacement autocorrelation function. Note that in the time domain the Bose-Einstein weight factor is equal to $-\ln[2\sinh(\pi t/\beta\hbar)]$ and reduces for long time t to $-\pi t/\beta\hbar$ at high temperatures and $\ln(\beta\hbar/2\pi t)$ at low. The time integration limit t_{max} is usually of the order of a few vibrational cycles and requires typically 25–35 time steps per cycle. All the integrals in our implementation of the EM method are evaluated using the trapezoidal rule, which is appropriate for highly oscillatory integrands.

B. Multiple scattering σ_j^2

Let us now apply the EM method to calculation of σ_j^2 for a general MS path. The sum of terms in Eq. (8) can be regrouped in the following way:

$$\sigma_j^2 = \left\langle\left[\sum_{i=1}^{n_j}\vec{u}_i\cdot\left(\frac{\hat{R}_{ii-}+\hat{R}_{ii+}}{2}\right)\right]^2\right\rangle. \tag{17}$$

Adopting a vector expansion of the displacements from Eq. (11), and evaluating the average using Bose-Einstein statistics [Eq. (13)], one can rewrite Eq. (17) as

$$\sigma_j^2 = \frac{\hbar}{2\mu_j}\sum_\lambda\frac{1}{\omega_\lambda}\coth\frac{\beta\hbar\omega_\lambda}{2}$$
$$\times\sum_i\left[\sqrt{\frac{\mu_j}{M_i}}\left(\frac{\hat{R}_{ii-}+\hat{R}_{ii+}}{2}\right)\cdot\vec{\epsilon}_i(\lambda)\right]^2. \tag{18}$$

The term in square brackets corresponds to the weight $|\langle\lambda|Q_j(0)\rangle|^2$ in Eq. (15) and can be interpreted as the normalized probability that the initial displacement state, i.e., the N-dimensional vector with only n_j nonzero components $|Q_j(0)\rangle \equiv |\sqrt{\mu_j/M_1}(\hat{R}_{1,n_j-}+\hat{R}_{1,2})/2,\ldots,\sqrt{\mu_j/M_i}(\hat{R}_{ii-}+\hat{R}_{ii+})/2,\ldots,0\rangle$ $(i=1,\ldots,n_j)$, is in vibrational mode $|\lambda\rangle = |\vec{\epsilon}_1(\lambda),\ldots,\vec{\epsilon}_N(\lambda)\rangle$. Here μ_j is defined so that $\langle Q_j(0)|Q_j(0)\rangle = 1$, which forces the projected VDOS $\rho_j(\omega)$ to be unit normalized:

$$\frac{1}{\mu_j} \equiv \sum_{i=1}^{n_j}\frac{1}{M_i}\left(\frac{\hat{R}_{ii-}+\hat{R}_{ii+}}{2}\right)^2. \tag{19}$$

For example, in the special case of SS the EM initial displacement state is defined as $|Q_R(0)\rangle \equiv |-\sqrt{\mu_R/M_0}\hat{R},\sqrt{\mu_R/M_R}\hat{R},0,\ldots\rangle$, where $\mu_R = (1/M_R+1/M_0)^{-1}$ is the reduced mass for the $(\vec{0},\vec{R})$ bond pair.

In order to simplify Eq. (18) one can define a normalized, local VDOS $\rho_j(\omega)$ as in Eq. (15), which leads to the frequency domain formula for MS σ_j^2 in Eq. (14). The VDOS spectrum $\rho_j(\omega)$ can be interpreted as the ''sound'' of the lattice plucked along the displacement vectors given by the initial conditions.

C. Force field models

The EM formalism presented above gives a relation between XAFS DW factors and the local microscopic environment around the scattering center. In order to apply the method, knowledge of the local force field model describing effective interatomic interactions or dynamical matrix D is required. Clearly, the choice of the model depends on the type of the interatomic bonds. For practical considerations the model should be kept as simple as possible: i.e., the number of its independent parameters should be small yet sufficient to avoid unphysical zero-frequency modes and to have an accuracy to within a few percent.

One commonly used model is the VFF model[14] which expresses energy changes in terms of changes in ''internal coordinates'' such as bond lengths $\delta r_{ij}=(\vec{u}_i-\vec{u}_j)\cdot\hat{R}_{ij}$, bond angles $\delta\theta_{ijk}$, etc. The potential energy of the lattice deformation in this case can be written as a quadratic form

$$\Phi=\frac{1}{2}\sum k_r^{ij}(\delta r_{ij})^2+\frac{1}{2}\sum k_\theta^{ijk}(\delta\theta_{ijk})^2+\cdots . \quad (20)$$

Here k_r^{ij} is a bond-stretching force constant for nearest neighbors i and j, k_θ^{ijk} is a bond-bending force constant corresponding to an angular rigidity for the angle θ_{ijk}, and the remaining terms are due to contributions from noncentral interactions proportional to products of changes in different internal coordinates, e.g., $(\delta r_{ij})\times(\delta r_{jk})$, $(\delta r_{ij})\times(\delta\theta_{ijl})$, etc. Because interatomic bonds are crucial for describing interactions in molecules and covalent crystals, the VFF model is particularly effective for such structures. An advantage of the model is that the dependence of the deformation energy solely on deformations of the bonds makes it rotationally invariant. For some materials (e.g., copper crystal) only a single near-neighbor force constant is needed to approximate most of the structure in vibrational spectra and to obtain σ_j^2 in good agreement with experiment. Sometimes it is more convenient to introduce effective central interactions with further neighbors rather than using bond angles and/or cross terms, although such interactions may not correspond to ''real'' chemical bonds. There exist a large number of other prescriptions for treating lattice deformations. These include the Born[15] and Keating[16] models which are used primarily for diamond-type crystals. In any case, the first near-neighbor central force constants are usually the largest in the interaction picture. In the future, however, it would be desirable to calculate these force constants by an *ab initio* method.

In the present paper we will not consider effects arising from anharmonic corrections to the potential energy. In general, anharmonicity leads to interactions between the various modes, and gives a contribution to $\sigma_j^2(T)$ that increases with temperature. Further discussions on this topic can be found elsewhere.[4,17–19] Due to anharmonic effects, the Gaussian approximation for DW factor Eq. (1) is not precisely valid, and the general cumulant expansion[3,4] has to be considered instead.

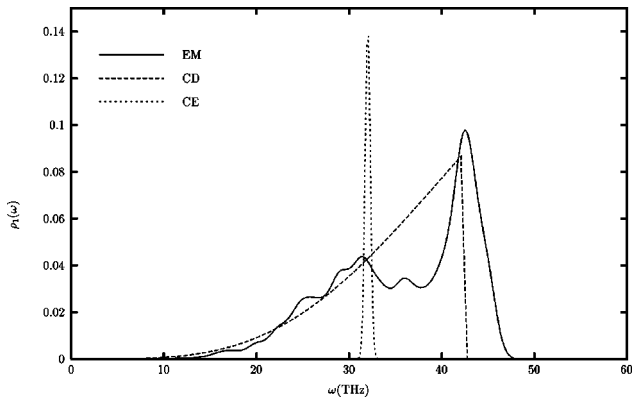

FIG. 1. Projected VDOS $\rho_R(\omega)$ for the first shell of Cu calculated using the EM method with $N=459$ and $k_1=27.9$ N/m (solid line), in comparison with CD (long dashed line) and CE (short dashed line) models.

D. Correlated Debye and Einstein models

In this subsection we will briefly review the standard CD and CE models often adopted for approximating XAFS DW factors and which are used for comparison with EM method in Sec. III. The CD model is essentially a spherical approximation to σ_R^2 in terms of the eigenmodes [Eq. (20)] and leads to a projected VDOS for an atomic bond $(\vec{0},\vec{R})$ of the form[5]

$$\rho_R(\omega)=\frac{3\omega^2}{w_D{}^3}\left[1-\frac{\sin(\omega R/c)}{\omega R/c}\right]. \quad (21)$$

Here $\omega_D=k_B\theta_D/\hbar$ is the Debye frequency, θ_D is the Debye temperature, $c=\omega_D/k_D$ is the Debye approximation for the speed of sound, $k_D=(6\pi^2N/V)^{1/3}$, and N/V is the atomic density number in the crystal. The second term in the brackets accounts for correlations and depends on bond length.

The CE model approximates the vibrational spectrum with a single δ function centered at the effective vibrational frequency $\omega_E(R_j)$, which in general, depends on the path of interest:

$$\rho_j(\omega)=\delta(\omega-\omega_E(R_j)). \quad (22)$$

The Einstein frequency $\omega_E(R_j)$ for the XAFS DW factor for scattering path j can be interpreted in terms of the local potential energy in the deformed lattice state $|Q_j(0)\rangle$, i.e., $\omega_E^2(R_j)=\langle Q_j(0)|D|Q_j(0)\rangle$. In the SS case, for example, $\omega_E(R)$ is related to the local effective bond-stretching force constant $k_R=\mu_R\omega_E^2(R)$. This value of $\omega_E(R)$ is equivalent to the ''natural'' vibrational frequency of the bond $(\vec{0},\vec{R})$ *together* with all attached neighboring bonds, but regarding all other masses as fixed.[17,18] Similarly, for a MS path j the potential energy $(1/2)k_j\sigma_j^2$ of a stretched path j with path length fluctuation $2\sigma_j$ is equal to that of a single-spring model with reduced mass μ_j [see Eq. (19)] and spring constant $k_j\equiv\mu_j\omega_E^2(R_j)$. The CE model is particularly appropriate for materials with $\rho_j(\omega)$ sharply peaked around a single

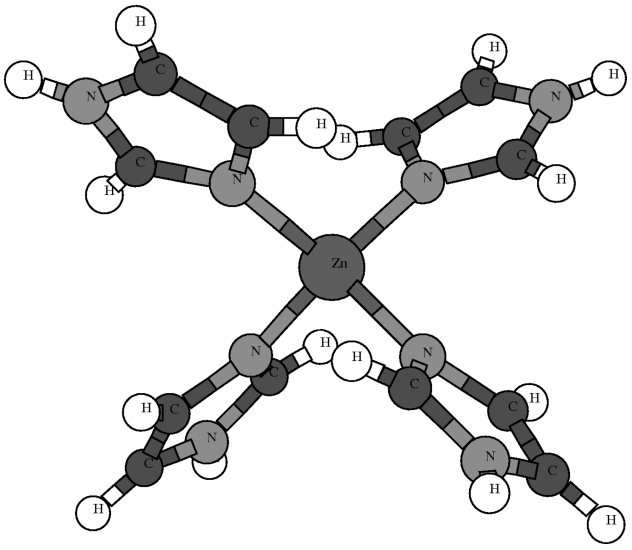

FIG. 2. Structure of the 37-atom zinc tetraimidazole macromolecule based on the coordinates given by LPT (Ref. 16).

frequency, but otherwise has most of the advantages and disadvantages of the CD model.

In general, depending on the form of the vibrational spectra, one or the other of these phenomenological models may provide a better approximation, but neither is usually adequate for heterogeneous systems. Plots of projected VDOS $\rho_R(\omega)$ for the first shell of Cu calculated using our nonisotropic EM method ($k_1=27.9$ N/m), the CD ($\theta_D=327$ K) and CE ($\theta_E\equiv\hbar\omega_E/k_B\simeq 3/4\theta_D\simeq 245$ K) models are presented in Fig. 1. The value $\theta_D=327$ K was obtained from a fit to experimental XAFS data (see Sec. III B).

III. APPLICATIONS

A. DW factors for zinc tetraimidazole

The study of the vibrational and dynamical properties of complex organic structures such as zinc tetraimidazole is complicated by a large number of degrees of freedom and a corresponding number of force constants. Imidazole is a crucial organic compound occurring in nucleic acid bases and amino acids, e.g., is an important constituent of the amino acid histidine. We chose zinc tetraimidazole since it was studied in detail by Loeffen, Pettifer, and Tomkinson[20] (LPT) and thus permits quantitative comparisons. This macromolecule consists of four imidazole ring molecules ($N_2C_3H_4$) attached to a zinc atom, forming a slightly distorted tetrahedral structure (Fig. 2). The entire cluster has C_2 point symmetry group with the zinc atom lying on a twofold axis and includes 37 atoms. To obtain all the parameters describing the force field of such complex materials is rarely possible, and therefore it is crucial for XAFS analysis to have a simplified prescription for calculating DW factors using a minimum set of parameters.

As a basis for the EM calculations we started with the full harmonic force field deduced from inelastic neutron scattering of natural and deuterated zinc tetraimidazole compounds.[20] This force field is essentially a VFF with deformations described in terms of combinations of internal coordinates such as bond stretches, angle bends, and torsions, and contains more than 60 distinct force constants, 40 of which correspond to internal vibrations of the imidazole branches. As may be guessed from the geometry of the structure, these internal modes, as well as the ''flapping'' modes of the branches, have little effect on the radial vibrations of the Zn-N bonds that dominate σ_1^2. Thus, by simplifying the VFF of the imidazole units, the number of the parameters used in the calculations can be significantly reduced without causing large errors in σ_1^2. Because torsional force constants are two orders of magnitude smaller than the dominant stretches, we neglected their effects in our simulations altogether. Several other negligibly small force constants were omitted as well. Our study consists of three steps in building a model structure analogous to that of LPT. Starting with a simple five-atom cluster, we then gradually add more degrees of freedom. At the first two steps, averages of the several similar force constants were used rather than their slightly different fitted values, which further reduced the number of parameters. We refer the reader to the paper by LPT for detailed definitions of the internal coordinates (i.e., bonds and angles). The numerical implementation of our method was successfully checked by comparing EM calculations of frequency modes with those calculated analytically by applying a group theoretic analysis to a tetrahedral XY_4 model with three force constants: bond stretching, angle bending, and bond coupling.

(1) As a starting model [Fig. 3(a)] we considered a five-atom cluster consisting of a zinc atom in the center surrounded by four pseudoatoms $\tilde{N}$ with masses equal to the mass of the imidazole ring (68 u). The geometry of the cluster was kept the same as in the ZnN_4 group of the original structure. Only two force constants were used in the calculation: a bond stretching k_0 (degeneracy 4) and an angle bending θ_0 (degeneracy 6) (see Table I). The first parameter was set equal to the average of the two Zn-N stretches in the full VFF of LPT, and the latter to the average of the four N-Zn-N angle bends (taking into account degeneracy due to

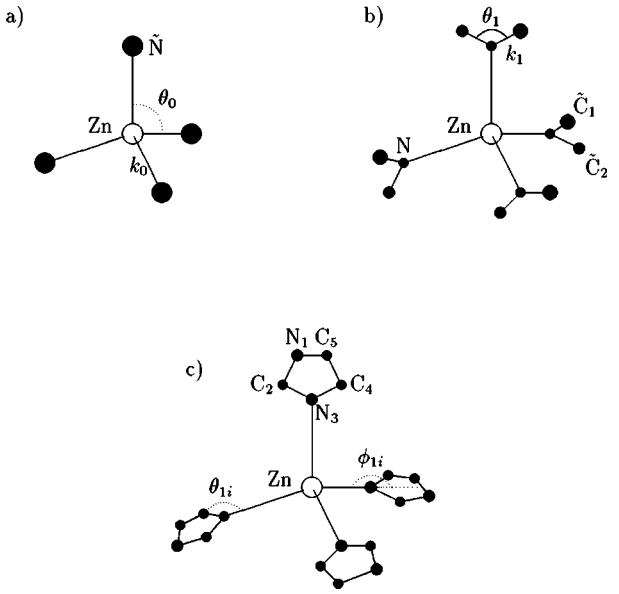

FIG. 3. Reduced structural models used to approximate the VFF of zinc tetraimidazole with (a) two and (b) four effective force constants, as well as (c) the 23-parameter VFF.

TABLE I. Force constants used in our VFF models for σ_j^2 calculation in zinc tetraimidazole. The first four parameters were used in models 1 and 2 and the remainder in model 3. Here $\tilde{N}$ and $\tilde{C}$ are pseudoatoms (see text). All angle bends are scaled by corresponding near-neighbor distances.

Symbol	Description	Value (N/m)
k_0	Zn–$\tilde{\text{N}}$ stretch	110
θ_0	$\tilde{\text{N}}$–Zn–$\tilde{\text{N}}$ bend	37
k_1	N–$\tilde{\text{C}}$ stretch	626
θ_1	$\tilde{\text{C}}$–N–$\tilde{\text{C}}$ bend	2590
$k_0^{(A)}$	Zn–N stretch	111
$k_0^{(B)}$	Zn–N stretch	108
α	Zn–N/Zn–N	27.4
β	Zn–N/Zn–N	3.77
θ_{01}	N–Zn–N bend	46.1
θ_{02}	N–Zn–N bend	26.1
θ_{03}	N–Zn–N bend	40.9
θ_{04}	N–Zn–N bend	21.8
ϕ_{11}	imid out-of-plane bend	9.0
ϕ_{12}	imid out-of-plane bend	7.3
k_{11}	N_1–C_2 stretch	670
k_{12}	N_1–C_5 stretch	681
k_{13}	C_4=C_5 stretch	561
k_{14}	N_3–C_4 stretch	500
k_{15}	N_3=C_2 stretch	752
γ_1	N_1–C_2/N_1–C_5	47.3
γ_2	N_1–C_5/C_4=C_5	45.0
γ_3	C=$_4C_5$/N_3–C_4	25.4
γ_4	N_3–C_4/N_3=C_2	81.1
θ_{11}	Zn–N–C bend	10.9
θ_{12}	Zn–N–C bend	14.8
ζ_A	ring deformation	260
ξ_B	ring deformation	250

the symmetry). The model yielded SS $\sigma_1^2 = 2.06\times10^{-3}$ Å^2 at 20 K, about 18% below the value estimated from experimental XAFS data, $(2.5\pm0.2)\times10^{-3}$ Å^2.

(2) In the second, slightly bigger calculation, we included the ZnN_4 group and eight pseudoatoms in place of the carbon atoms nearest to the nitrogens [see Fig. 3(b)]. Four of these pseudoatoms ($\tilde{C}_1$) had masses equal to the sum M(C) $+M$(N)$+2M$(H)$\simeq$28. u and the other four ($\tilde{C}_2$) to $2[M(\text{C}+M(\text{H})]\simeq$26. u. Four force constants were used in the calculation (see Table I): in addition to the two parameters of model (1) we considered a stretch k_1 between the nitrogen and the $\tilde{C}_i$ nearest to it equal to the average of the two N-C stretches and an angle bending θ_1 (the result of the combining two ring deformations and calculating coefficients at the corresponding angle bend term). For the short Zn-N bond the resulting $\sigma_1^2 = 2.43\times10^{-3}$ Å^2 at 20 K.

(3) Finally, we included all atoms of the imidazole units except the hydrogens [see Fig. 3(c)] and used 23 distinct force constants in the VFF model: two Zn-N bond stretches $k_0^{(A)}$ and $k_0^{(B)}$, two Zn-N bond couplings α and β, six skeletal angle bends θ_{0i}, two out-of-plane angle bends of the imidazole branches ϕ_{1i}, five bond stretches inside the imidazole rings k_{1i}, four imidazole bond couplings γ_i, and two ring-deformation constants ζ_A and ξ_B. The result for the weaker (108 N/m) Zn-N bond is $\sigma_1^2(20\text{ K}) = 2.64\times10^{-3}$ Å^2, in good agreement with the value obtained by LPT (2.62×10^{-3} Å^2). For the stronger (111 N/m) bond the EM calculation yielded 2.63×10^{-3} Å^2, again in excellent agreement with the values calculated by LPT (2.60×10^{-3} Å^2).

We also used these three models to calculate σ_j^2(20 K) for four MS triangular paths of the type Zn$\rightarrow N^{(1)}\rightarrow N^{(2)}\rightarrow$Zn where $N^{(1)}$ and $N^{(2)}$ are the nearest neighbors to the scattering center (see Table II). Note a significant effect of the $N^{(1)}$-Zn-$N^{(2)}$ bending force constants and geometry on the σ_j^2 values. The wider the angle, the greater the resistance to its deformation, and hence these σ_j^2's are inversely proportional to φ_j. The values of σ_j^2 appear to be rather large since there is no explicit N-N stretching involved.

These results (Table III) show that, due to the local nature of σ^2, it is possible to reduce dramatically the number of the parameters in the VFF even for very complex structures while still attaining a 5–10% accuracy in the final results for σ^2 in comparison with both more precise theory and experimental data. This accuracy is satisfactory, since the error bars for the force constants themselves are usually of the same order, e.g., about 15% for Zn-N bond-stretching constants in zinc tetraimidazole, and the accuracy of the EM method, as implemented in our code, is fixed to be about 5%.

The vibrational spectrum of the zinc tetraimidazole molecule can be subdivided into high- and low-frequency regimes. The high-frequency regime (>500 cm^{-1}) corre-

TABLE II. Values of MS σ_j^2 at 20 K calculated for four central MS paths of the type $\text{Zn}\xrightarrow{k^{(1)}}N^{(1)}\xrightarrow{\theta}N^{(2)}\xrightarrow{k^{(2)}}\text{Zn}$ in zinc tetraimidazole depending on the number of the force constants (ν) used in the VFF model. Here j is the MS path index, R_j its effective length, φ_j the scattering angle $N^{(1)}$-Zn-$N^{(2)}$ in degrees, $k^{(i)}$ the force constant for the bond Zn-$N^{(i)}$, and θ is the bending force constant for the corresponding φ_j. All force constants are given in N/m.

			σ_j^2 (10^{-3} Å^2)					
j	R_j (Å)	φ_j	$\nu=2$	4	2	$k^{(1)}$	$k^{(2)}$	θ 3
19	3.57	107	3.17	4.10	3.94	108	111	40.9
20	3.59	108	3.17	4.71	4.95	111	111	26.1
21	3.62	111	3.16	4.05	3.86	108	111	46.1
22	3.63	112	3.15	4.47	4.87	108	108	21.8

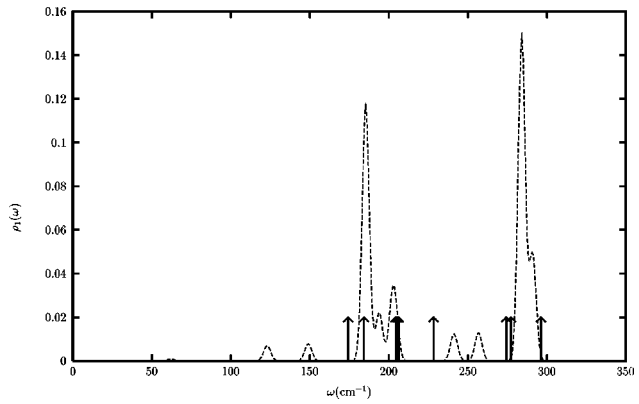

FIG. 4. Low-frequency part of the first shell projected VDOS $\rho_R(\omega)$ for the 23-parameter model of Zn tetraimidazole ($N=21$). The lines at 296, 277, 274, 228, 206, 205, 204, 184, and 174 cm^{-1} indicate low-frequency tetrahedral modes obtained by LPT (Ref. 16) for the entire 37-atom macromolecule.

sponds to the modes caused by internal motion of the imidazole branches, while the low-frequency regime (<500 cm^{-1}) consists of skeletal vibrational modes such as tetrahedral deformations, and in- and out-of-plane librations of the imidazole branches. These low-frequency modes yield almost 70% of the calculated σ_1^2. The low-frequency part of the projected VDOS for the Zn-N bond (first shell) is presented in Fig. 4. The peaks lying in the range between 170 cm^{-1} and 300 cm^{-1} correspond to the tetrahedral modes, whereas the lower part of the spectrum is due to the librations of the imidazole branches. Due to the small size of the system, the spectra are highly discrete. For such heterogeneous materials like zinc tetraimidazole, a single-parameter CD or CE model is not accurate.

TABLE III. Values of SS σ_1^2 at 20 K for the weak Zn–N bond in zinc tetraimidazole depending on the number of the force constants (ν) used in the VFF model. Here $\epsilon_{\mathrm{expt}}=100(\sigma_1^2-\sigma_{\mathrm{expt}}^2)/\sigma_{\mathrm{expt}}^2$ and $\epsilon=100(\sigma_1^2-\sigma_{\mathrm{LPT}}^2)/\sigma_{\mathrm{LPT}}^2$ with $\sigma_{\mathrm{expt}}^2=(2.5\pm0.2)\times10^{-3}$ Å^2 and $\sigma_{\mathrm{LPT}}^2=2.62\times10^{-3}$ Å^2.

ν	σ_1^2 (10^{-3} Å^2)	ϵ_{expt} (%)	ϵ (%)
2	2.06	18	21
4	2.43	3	7
23	2.64	6	1

B. DW factors for Cu

The first crystalline structure examined in our MS calculations was a 459-atom spherical cluster of a copper crystal with fcc lattice symmetry. Although our method was designed for general aperiodic systems, we chose fcc Cu since it has often been used as a test case for DW and other XAFS studies and accurate XAFS data are available. Following the model of Rehr and Alben,[6] only a single central interaction between the first nearest neighbors with force constant $k_1=27.9$ N/m was taken into account. Example results for the first shell SS path and for the 111 triangular MS path versus temperature are shown in Fig. 5 in comparison with the CD model ($\theta_D=327$ K) results calculated by the FEFF code, as well as with experimental data[21,22] and the CE model for the first shell ($\theta_E=245$ K). Our results for SS σ_R^2 are in excellent agreement (within 0.3% for the first and second shells, and within 3% for the third shell) with those obtained by Sevillano *et al.*[5] using full lattice dynamical calculations. Excellent agreement with experiment at lower temperatures is also reached. At higher temperatures, i.e., above 500 K, the error between our theory and experiment is likely due to anharmonic effects. The results for σ_j^2 indicate that at all temperatures, the CD model is in good agreement with the

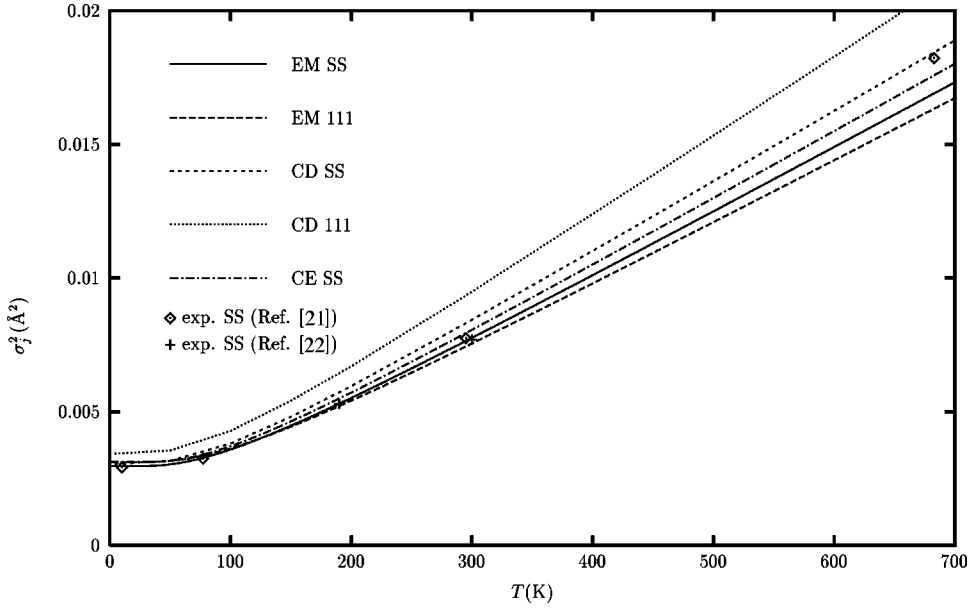

FIG. 5. Mean-square amplitudes σ_j^2 for a 459-atom cluster of Cu vs temperature as calculated from a single force constant ($k_1=27.9$ N/m) model for the first shell (EM SS) and for the 111 triangular MS path (EM 111). The CD model ($\theta_D=327$ K) calculations for the first shell (CD SS) and the 111 triangular MS path (CD 111) and the CE model for the first shell (CE SS) are given for comparison. Points represent experimental values of σ^2 (Refs. 21,22).

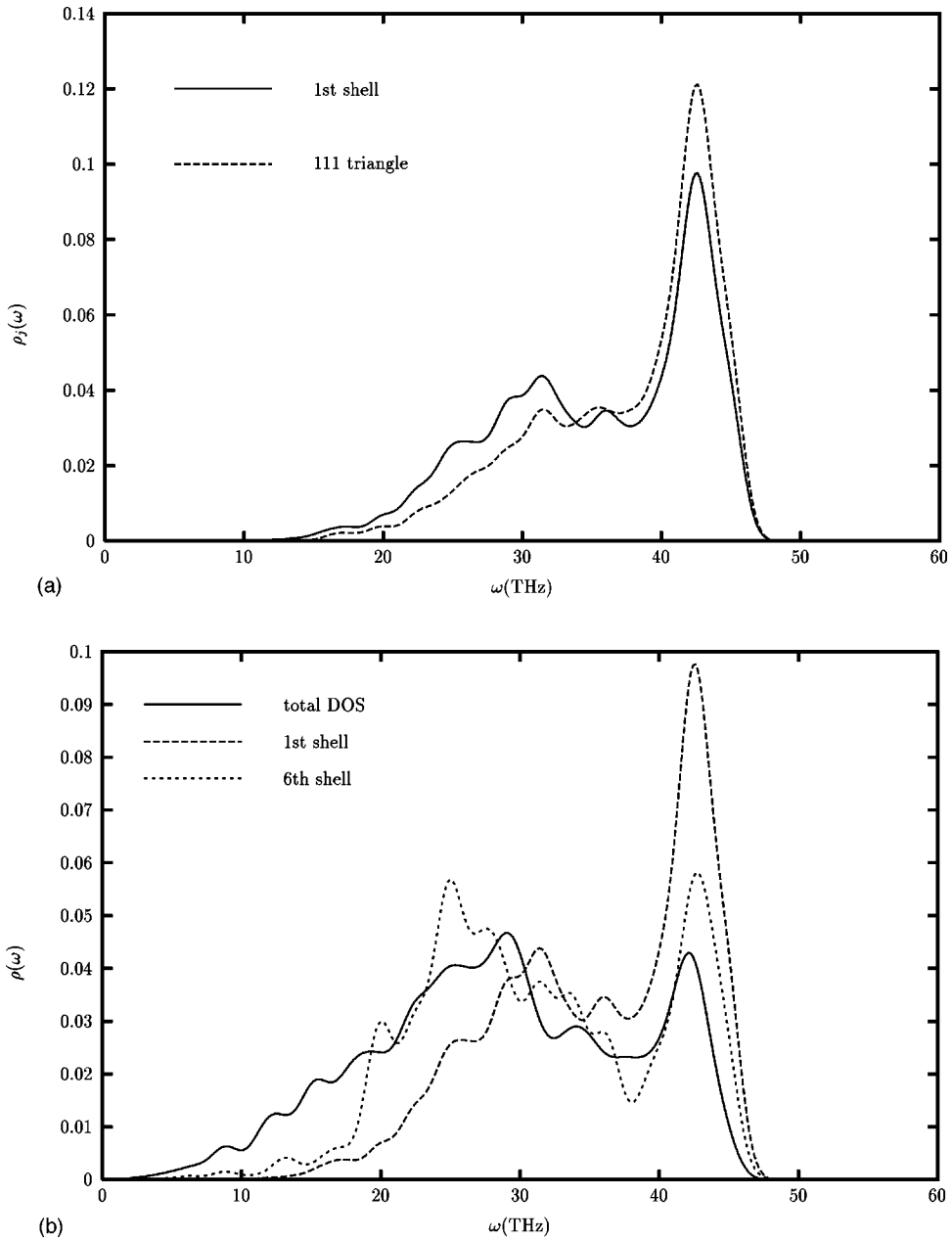

FIG. 6. (a) Projected VDOS $\rho_j(\omega)$ for the first shell (solid) and for the 111 triangular MS path (dashed line) for Cu calculated via EM method. (b) Total VDOS $\rho(\omega)$ and projected VDOS $\rho_R(\omega)$ for the first shell and sixth shells of Cu calculated via EM method.

EM method for the first shell SS path: i.e., the 10% difference is within the error bars of the two methods. A larger difference (about 25% at high temperatures) is observed for the 111 path. The discrepancies between the two models are smaller at low temperatures. Projected vibrational densities of states $\rho_j(\omega)$ for the two paths are shown in Fig. 6(a). Note that the VDOS for the 111 triangular path has a sharper dominant peak at about 42 THz; i.e., the $\rho_j(\omega)$ is more monochromatic for this path. One can think of it as the fine tone of a musical ''triangle.'' This feature also explains the bigger error in the CD $\sigma_j^2(T)$ for this path. Figure 6(b) illustrates the importance of correlations for nearest neighbors as well as the decay of the correlation function with distance. Note that the projected VDOS for the sixth shell is very similar to the total VDOS which indicates that contribution from the correlations is negligible for the further shells.

This study shows that overall the CD model is a reasonably good approximation for Cu, which might be expected since the fcc structure is highly isotropic. This also can be seen from a comparison of the XAFS Fourier transform $\tilde{\chi}(R)$ with fits of theoretical FEFF calculations using DW factors obtained via the CD model and the EM method (see Fig. 7). Fits of theoretical $\tilde{\chi}(R)$ to experiment measured at 150 K were performed using a phase-corrected version of FEFFIT, i.e., with theoretical phase shifts taken from FEFF7. As fitting parameters for the EM model we used a shift of energy origin ΔE and a constant amplitude factor S_0^2, whereas for the CD models we used ΔE and Debye temperature θ_D, and set S_0^2 equal to the value derived from the EM fit (0.927). The data were fitted in the range between 1.7 and 5.2 Å for the 16 most significant scattering paths which span the first four shells. The fitted value for θ_D was 327 ± 9 K,

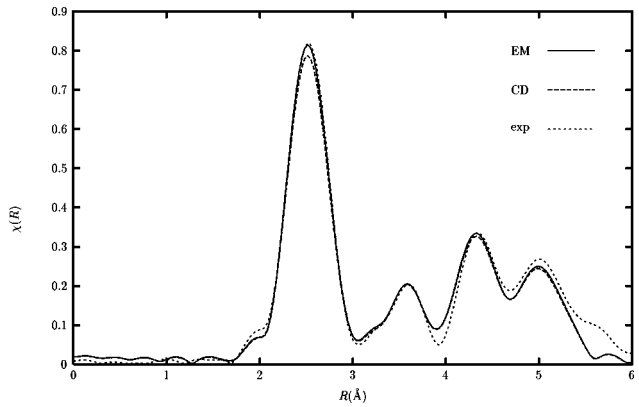

FIG. 7. Magnitude of the phase corrected Fourier transform $\tilde{\chi}(R)=\mathrm{FT}[k\chi(k)]$ for Cu at $T=150$ K as extracted from experiment using the phase corrected FEFFIT code (solid line), and fitted from theoretical results with DW factors calculated using CD (long dashed line) and single force constant EM (short dashed line) models.

within error bars of the value $\theta_D=315$ K.[23] As Fig. 7 shows, both methods yield XAFS in excellent agreement with experiment, though the EM method is noticeably better.

C. DW factors for Ge

The second crystal considered in our study was a 147-atom spherical cluster of Ge of the diamond space group. In the application of the EM method to such loose, anisotropic structures like Ge, a single-spring model is inadequate, and it is necessary to include noncentral forces to account for bond-bending interactions. Otherwise there is no resistance to shear, and the projected VDOS exhibits an unphysical zero-frequency mode. The force field model used in our calculations included central interactions out to the third neighbors ($k_1=120$ N/m for the first neighbors, 4.0 N/m for the second, and -1.1 N/m for the third), and noncentral bond-bending interactions[24] with $k_1^{nc}=0.04k_1$ fit to the experimental[25] VDOS. The values for the central interaction force constants were based on results of Goldammer *et al.*[26] and then adjusted by hand to fit the experimental spectrum determined from neutron scattering.[25] Figure 8 shows the calculated total and projected VDOS for this model in comparison with experimental total VDOS. The MS σ_j^2 at 300 K calculated by the EM method in comparison with results obtained from CD model [$\theta_D=360$ K (Ref. 23)] and several SS experimental values[22] are presented in Fig. 9 versus the scattering path index listed in order of increasing path length as generated by FEFF7. For example, path number 1 corresponds to first shell SS, 2 to second shell SS, 3 to 121 triangular MS path, 4 to triangular 211 MS path, 5 to third shell SS, 6 to double scattering from the first neighbor ($\sigma_6^2=4\sigma_1^2$), etc. According to the EM calculations for the first three paths, projected VDOS for paths 1 and 3 (see Fig. 8)

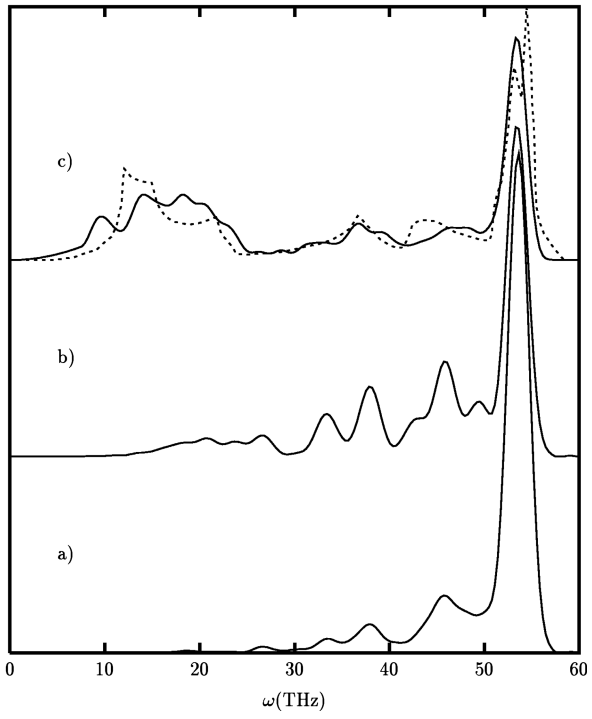

FIG. 8. VDOS for a 633-atom cluster of Ge as calculated via EM method (a) for the first shell and (b) for 121 triangular MS path. (c) Total experimental spectrum determined from neutron scattering (Ref. 26) in comparison with theoretical total VDOS $\rho(\omega)$.

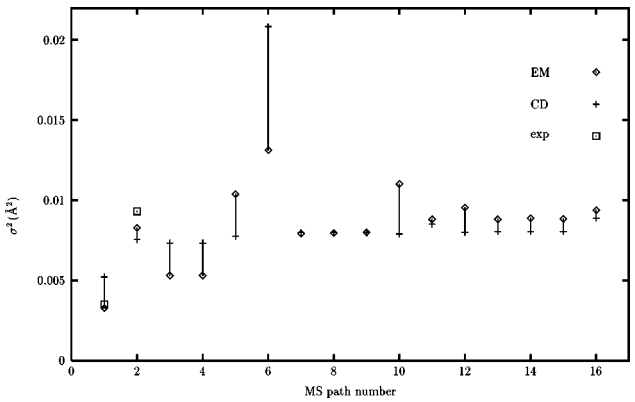

FIG. 9. XAFS MS σ^2 for 147-atom cluster of Ge as calculated with EM and CD models at $T=300$ K vs MS path index (see text). Two experimental values (Ref. 21), corresponding to the first and second shell SS, are given for comparison.

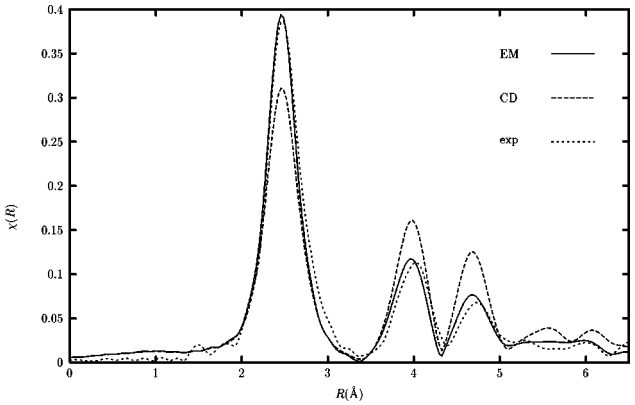

FIG. 10. Magnitude of the phase corrected Fourier transform $\tilde{\chi}(R)=\mathrm{FT}[k\chi(k)]$ for Ge at $T=300$ K as extracted from experiment using the phase-corrected FEFFIT code (solid line) and fitted from theoretical results with DW factors calculated using CD (long dashed line) and EM (short dashed line) models.

have sharper dominant optical peaks at about 50 THz whereas the VDOS for path 2 has a more smeared out spectrum and, thus, is probably better approximated with CD model. This explains the smaller difference with the CD model for path 2. The deficiency of the CD model for Ge is illustrated by the poor fit of the theoretical $\chi(R)$ to experimental XAFS spectra (see Fig. 10). Using the same fitting parameters as in the case of Cu above, the 300 K data were fitted in R space in the range between 2.0 and 5.2 Å for the 20 most significant scattering paths spanning the first five shells. The fitted value for θ_D was 375 ± 16 K, which again is within error bars from the value 360 K.[23]

IV. CONCLUSIONS

The EM method presented in this paper provides an efficient and general approach for the calculation of MS XAFS Debye-Waller factors in terms of local force constants. Our results illustrate a number of advantages of the EM method in comparison with traditional isotropic models, especially for heterogeneous materials which are those of greatest interest in XAFS studies. Due to the local nature of the DW factors, the method can be successfully applied to small and irregular structures by focusing on the vicinity of the scattering atom. It requires no symmetry specification or boundary conditions. Since no secular equations or matrix diagonalizations are involved and given the linear scaling of the numerical procedure with system size, the method is efficient even for clusters of more than several hundred atoms. In that case solving the ''exact'' eigenvalue problem is very time-consuming, since it scales as $(3N)^3$ for systems without symmetry where N is the number of atoms in the cluster. The real time approach to calculations of σ_j^2's using Eq. (16) shows that, in principle, it is not necessary to determine projected VDOS as an intermediate step which further simplifies the numerical computation. We have not used this approach in the present work since it is valuable to see the VDOS as well, and values of $\sigma_j^2(T)$ for any temperature T can be calculated once $\rho_j(\omega)$ is obtained. In fact, in many cases analysis of vibrational spectra may provide additional information for refining the dynamical model used in the EM method. Our study shows that isotropic models can be inaccurate not only for such highly inhomogeneous materials as biological complexes but even for some loosely packed monoatomic crystals like Ge. Our results also illustrate the importance of correlations in modeling vibrational properties of materials. The correlations decay with distance, and indicate how σ_j^2 converges to Σu_j^2. One of the most important features of the EM method is that given a local force field model with a few parameters one can calculate XAFS DW factors from first principles even when experimental data for ω_D or ω_E are not available or hard to extract, which is often the case for biological complexes. Finally, it would be desirable to have a general prescription for obtaining *ab initio* VFF model parameters in an efficient and reliable way, and we are currently exploring this possibility.

ACKNOWLEDGMENTS

We thank A. Ankudinov, T. Fujikawa, G. George, D. Haskel, M. Newville, P. Loeffen, B. Ravel, E. Stern, and N. Van Hung for many helpful discussions. We thank especially P. Loeffen for providing the VFF parameters for zinc tetraimidazole and M. Newville for providing the phase-corrected FEFFIT code and experimental XAFS data. This work was supported by Grant No. NIH RR 01209.

[1] E. A. Stern, in *X-Ray Absorption: Principles, Applications, Techniques of EXAFS, SEXAFS, and XANES*, edited by D. C. Konigsberger and R. Prins (Wiley, New York, 1988).
[2] S. I. Zabinsky, J. J. Rehr, A. Ankudinov, R. C. Albers, and M. J. Eller, Phys. Rev. B **52**, 2995 (1995). See also http://leonardo.phys.washington.edu/feff
[3] M. G. Newville, Ph.D. thesis, University of Washington, 1995.
[4] E. D. Crozier, J. J. Rehr, and R. Ingalls, in *X-Ray Absorption: Principles, Applications, Techniques of EXAFS, SEXAFS, and XANES*, edited by D. C. Konigsberger and R. Prins (Wiley, New York, 1988).
[5] E. Sevillano, H. Meuth, and J. J. Rehr, Phys. Rev. B **20**, 4908 (1979).
[6] J. J. Rehr and R. Alben, Phys. Rev. B **16**, 2400 (1977).
[7] G. Dalba and P. Fornasini, J. Synchrotron Radiat. **4**, 243 (1997).
[8] G. N. George, R. C. Prince, and S. P. Cramer, Science **243**, 789 (1989).
[9] M. Benfatto, C. R. Natoli, and A. Filipponi, Phys. Rev. B **40**, 9626 (1989).
[10] E. A. Stern, M. Newville, B. Ravel, Y. Yakoby, and D. Haskel, Physica B **208&209**, 117 (1995). See also http://leonardo.phys.washington.edu/uwxafs
[11] T. Fujikawa and J. J. Rehr, J. Synchrotron Radiat. (to be published).
[12] A. A. Maradudin, E. W. Montroll, G. H. Weiss, and I. P. Ipatova, *Theory of Lattice Dynamics in the harmonic Approximation*, 2nd ed. (Academic, New York, 1971).
[13] D. Beeman and R. Alben, Adv. Phys. **26**, 339 (1977).
[14] M. J. P. Musgrave and J. A. Pople, Proc. R. Soc. London, Ser. A **268**, 474 (1962).
[15] M. Born and K. Huang, *Dynamical Theory of Crystal Lattices* (Oxford University Press, New York, 1954), Chap. V.
[16] P. N. Keating, Phys. Rev. **145**, 637 (1966).
[17] A. I. Frenkel and J. J. Rehr, Phys. Rev. B **48**, 585 (1993).
[18] N. V. Hung and J. J. Rehr, Phys. Rev. B **56**, 43 (1997).
[19] T. Fujikawa, T. Miyanaga, and T. Suzuki, J. Phys. Soc. Jpn. **66**, 2897 (1997).
[20] P. W. Loeffen, R. F. Pettifer, and J. Tomkinson, Chem. Phys. **208**, 403 (1996).
[21] R. B. Greegor and F. W. Lytle, Phys. Rev. B **20**, 4902 (1979).
[22] E. A. Stern, B. A. Bunker, and S. M. Heald, Phys. Rev. B **21**, 5521 (1980).
[23] N. W. Ashcroft and N. D. Mermin, *Solid State Physics* (Holt, Rinehart and Winston, New York, 1976).
[24] R. Alben, D. Weaire, J. E. Smith, and M. H. Brodsky, Phys. Rev. B **11**, 2271 (1974).
[25] M. F. Thorpe, Phys. Rev. B **15**, 5352 (1973).
[26] W. Goldammer, W. Ludwig, and W. Zierau, Phys. Rev. B **36**, 4624 (1987).